

Selective dynamic band gap tuning in metamaterials using graded photoresponsive resonator arrays

*Original*

Selective dynamic band gap tuning in metamaterials using graded photoresponsive resonator arrays / Dal Poggetto, V.F., Urban, D., Nistri, F., Beoletto, P.H., Descrovi, E., Miniaci, M., Pugno, N.M., Bosia, F., Gliozzi, A.S.. - In: PHILOSOPHICAL TRANSACTIONS OF THE ROYAL SOCIETY OF LONDON SERIES A: MATHEMATICAL PHYSICAL AND ENGINEERING SCIENCES. - ISSN 1364-503X. - 382:2279(2024). [10.1098/rsta.2024.0150]

*Availability:*

This version is available at: 11583/2991945 since: 2024-08-26T15:45:13Z

*Publisher:*

Royal Society

*Published*

DOI:10.1098/rsta.2024.0150

*Terms of use:*

This article is made available under terms and conditions as specified in the corresponding bibliographic description in the repository

*Publisher copyright*

(Article begins on next page)



**Subject Areas:**

xxxxx, xxxxx, xxxxx

**Keywords:**

Metamaterials, tunability, graded resonators, photoresponsive materials, band gaps

**Author for correspondence:**

Antonio S. Glozzi

e-mail: [antonio.glozzi@polito.it](mailto:antonio.glozzi@polito.it)

# Selective dynamic band gap tuning in metamaterials using graded photoresponsive resonator arrays

V. F. Dal Poggetto<sup>1,4</sup>, D. Urban<sup>2,3</sup>, F. Nistri<sup>3</sup>, P. H. Beoletto<sup>3</sup>, E. Descrovi<sup>3</sup>, M. Miniaci<sup>1</sup>, N. M. Pugno<sup>4,5</sup>, F. Bosia<sup>3</sup>, A. S. Glozzi<sup>3\*</sup>

<sup>1</sup> Univ. Lille, CNRS, Centrale Lille, Junia, Univ. Polytechnique Hauts-de-France, UMR 8520 Lille, France

<sup>2</sup> Department of Electronic Systems, Norwegian University of Science and Technology, 7491 Trondheim, Norway

<sup>3</sup> DISAT, Politecnico di Torino, 10129 Torino, Italy

<sup>4</sup> Laboratory for Bioinspired, Bionic, Nano, Meta Materials & Mechanics, Department of Civil, Environmental and Mechanical Engineering, University of Trento, Trento, 38123 Italy

<sup>5</sup> School of Engineering and Materials Science, Queen Mary University of London, UK

The introduction of metamaterials has provided new possibilities to manipulate the propagation of waves in different fields of physics, ranging from electromagnetism to acoustics. However, despite the variety of configurations proposed so far, most solutions lack dynamic tunability, i.e., their functionality cannot be altered post-fabrication. Our work overcomes this limit by employing a photoresponsive polymer to fabricate a simple metamaterial structure and enable tuning of its elastic properties using visible light. The structure of the metamaterial consists of graded resonators in the form of an array of pillars, each giving rise to different resonances and transmission band gaps. Selective laser illumination can then tune the resonances and their frequencies individually or collectively, thus yielding many degrees of freedom in the tunability of the filtered or transmitted wave frequencies, similar to playing a keyboard, where illuminating each pillar corresponds to playing a different note. This concept can be used to realize low-power active devices for elastic wave control, including beam-splitters, switches, and filters.

© The Authors. Published by the Royal Society under the terms of the Creative Commons Attribution License <http://creativecommons.org/licenses/by/4.0/>, which permits unrestricted use, provided the original author and source are credited.

## 1 Introduction

Elastic and acoustic metamaterials derive unconventional dynamic properties from the combined behavior of artificial structural elements [1–3]. Generally speaking, metamaterial functionality depends mainly on unit cell design, but material properties play a role in determining the frequencies at which these effects take place. To date, elastic and acoustic metamaterials exploit three main distinct mechanisms for the control of wave propagation: (i) Bragg scattering, (ii) local resonances, and/or (iii) inertial amplification [4, 5]. The wave manipulation effects that can be achieved with these mechanisms include elastic wave scattering [6], acoustic wave absorption [7], negative refraction [8], cloaking [9], focusing [10], one-way [11] or scatter-free propagation [12], and topological protection [13]. These effects can be exploited for numerous applications across scales, from isolation of large scale vibrations [14–16] to energy harvesting [17], from noise abatement [18, 19] to speech recognition [20].

Despite their scientific interest and their numerous applications, most elastic and acoustic metamaterials lack dynamic tunability, i.e., their functionality is fixed once the structure has been fabricated. To address this limitation, the coupling of metamaterials with different external fields, such as piezoelectric [21–25], thermal [26–28], mechanical (prestress/prestrain) [29–32], and electromagnetic [33–38] ones, has been explored. Alternative approaches include the use of soft magnetoactive composites exploiting instabilities [39, 40], strain-tunable dielectric elastomers [41] or magnetorheological metamaterials exploiting nonlinear effects [42], leading to the concept of “soft, smart matter” [43].

However, practical implementations often involve considerable complexity, both in specimen fabrication and in the implementation of the control mechanism. In contrast, here we propose an approach that exploits light responsiveness into a 3D printable polymeric material, enabling simple, non-contact and low-power tunability [44].

In previous work, we have demonstrated the controlled decrease of the Young’s modulus of polymers containing azobenzene dye by means of laser illumination and the corresponding modification of the transmission properties of a metamaterial structure fabricated with this material and consisting in an array of pillars on a waveguide. Selective local illumination affects the vibration eigenmodes of individual resonant pillars, significantly affecting the waveguide transmission spectrum [45, 46]. These effects occur on a time scale of less than a minute and are fully reversible. In this work, we present a continuation of previous investigations, extending the analysis to graded structures, thus allowing to increase the possible degrees of freedom in tunability of the system, and conceptually introducing the possibility of “playing” a metamaterial keyboard.

## 2 Specimen design and numerical analysis

In a system consisting of multiple photoresponsive pillars of identical heights on a waveguide (see Fig.1a), each pillar exhibits a similar dynamic behavior, eigenfrequencies (schematically shown in Fig.1b) and eigenmodes. When excited at their resonant frequencies, they collectively generate a band gap with a specific centre frequency and width. If one of these pillars is selectively illuminated, its resonance frequency decreases (since the material undergoes softening), causing the band gap to move to lower frequencies (Fig.1c) [46]. On the contrary, in a scenario where each pillar has a different height (Fig.1d), the resonant frequencies also differ, resulting in individual pillars attenuating the propagation of waves around different centre frequencies (Fig.1e). This system is reminiscent of the so-called “resonant metawedge”, which has been extensively discussed in various contexts of elastic wave manipulation [14, 17]. In our case, when one of the photo-responsive pillars is illuminated, the corresponding band gap width remains approximately the same but shifts towards lower frequencies (Fig.1f). This behavior, together with the selective illumination of one or more graded pillars, enables the tunability of the transmission properties of the entire structure.

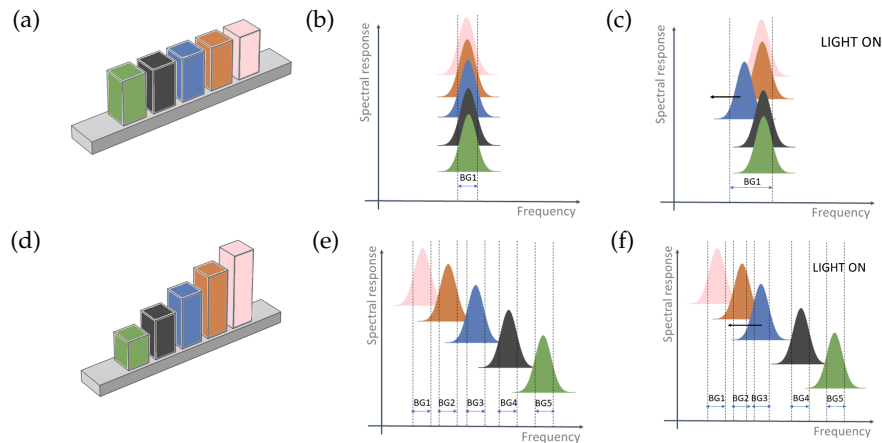


Figure 1: Schematic representation of the proposed concept: a) pillar array acting as a metamaterial filter; b) the local resonance properties of all pillars coincide and lead to a single band gap (BG1) at a characteristic frequency; c) laser illumination of a single photoresponsive pillar leads to a downward shift of its resonance, and an overall widening of the bandgap. d) In this work, we consider an array of pillars of variable height, whose spectral response is given by e) the superposition of resonances at different frequencies, i.e. various potentially overlapping bandgaps; f) illumination of a single pillar allows manipulation of the filtering properties in a specific frequency range.

To guide the design of the resonator arrays, a first numerical investigation on the modal properties of the individual pillars is performed. **The system can be considered as an array of subwavelength resonators that can trap and spatially segregate certain frequencies, when the traveling waves in the beam efficiently couple with the pillar resonances, i.e., an impedance matching condition occurs. To determine this condition, we** calculate the dispersion spectra of the individual pillars and their resonance frequencies as a function of their height. We design the array so that there is no overlap between the lowest bandgaps of the different pillars, identifying four distinct pillar heights that satisfy this condition.

The dispersion spectrum of the resonator array, whose unit cell is shown in Fig.2(a) with its characteristic dimensions (a hosting base of width  $a$  and height  $h_b$ , supporting a pillar of width  $b$  and height  $h_p$ ), is computed using Finite Element (FE) analysis. The models are meshed using quadratic hexahedral solid elements (nodal displacements  $u_x$ ,  $u_y$ , and  $u_z$ ) with a characteristic length of approximately 0.5 mm. Material properties are considered homogeneous and isotropic, with a Young's modulus value 2.75 GPa, Poisson's ratio 0.3, and specific mass density  $1120 \text{ kg} \cdot \text{m}^{-3}$ . Bloch-Floquet periodic conditions are enforced at the edges of the one-dimensional unit cell in the  $x$ -direction [47], resulting in an eigenproblem in the form  $\mathbf{K}(k)\mathbf{u} = \omega^2 \mathbf{M}\mathbf{u}$ , where  $\mathbf{K}(k)$  is a wavenumber-dependent stiffness matrix,  $\mathbf{M}$  is a mass matrix,  $\omega^2$  are the eigenvalues which correspond to propagating frequencies, and  $\mathbf{u}$  are the eigenvectors which represent the nodal three-dimensional displacements. This eigenproblem is solved by considering the wavenumber  $k$  within the corresponding irreducible Brillouin zone [48], spanning the values between the points  $\Gamma(k=0)$  and  $X(k=\pi/a)$ , since we are considering 1D propagation along a waveguide. Additionally, an out-of-plane polarization metric [49] expressed by  $p(\mathbf{u}) = (\int_V |u_z|^2 dV) / (\int_V |u_x|^2 + |u_y|^2 + |u_z|^2 dV)$ , with  $p \in [0, 1]$ , is computed for the subset of displacement vectors  $\mathbf{u}$  considering the volume of the hosting beam (region marked in blue in Fig.2(a)), which we consider as indicative of the flexural behavior of the beam in the experimental setup. For the considered values of  $a = 5 \text{ mm}$ ,  $h_b = 2 \text{ mm}$ , and  $b = 3.75 \text{ mm}$ , the dispersion relations are computed for the heights  $h_p$  of (i) 7 mm, (ii) 9 mm, (iii) 11 mm, and (iv) 13 mm, and shown in Fig.2(b) along with the computed polarization values ( $p$ ) for the propagating

frequencies of a branch that presents significant coupling between the in- and out-of-plane motion of the hosting beam. This behavior is illustrated for  $h_p = 7$  mm by the wave modes computed at  $\Gamma_1$ ,  $P_1$  ( $k = \pi/2a$ ), and  $X_1$ , which display, respectively, the propagating frequencies of 45.1, 50.6, and 71.3 kHz. The polarization values of these points are 0.70, 0.54, and 0.10, indicating a predominantly out-of-plane behavior for the hosting beam at  $\Gamma_1$  and in-plane at  $X_1$ . On the other hand, the wave mode at  $P_1$  presents a high degree of coupling between the in- and out-of-plane behavior of the hosting beam, which is also observed on the combined motion of the supported pillar (see wave mode in Fig.2(b)). The out-of-plane behavior of the hosting beam at  $\Gamma_1$  suggests that corresponding peaks will arise in the transmission of a finite structure formed by these unit cells for an out-of-plane excitation. The polarization values decrease monotonically in this branch, thus suggesting that for a continuous frequency range, a coupled behavior between in- and out-of-plane motion is expected, which in turn, may yield a reduction in the transmission of out-of-plane excitation due to coupling with the pillar motion. A similar behavior is observed for each case of the pillar height, as shown in the dispersion spectra in Fig.2(b). The propagating frequencies of the corresponding branches at  $\Gamma$  for the pillar heights of 9, 11, and 13 mm are respectively 33.6, 25.9, and 20.5 kHz, thus indicating a trend of decrease in the propagating frequencies as the pillar height increases. We also expect these points to be associated with peaks in the transmission of out-of-plane excitation in a finite system. Interestingly, a shift in the computed frequencies can be achieved through the variation of the pillar height while maintaining a fixed lattice length, therefore indicating the prevalently locally resonant nature of the wave modes. The corresponding polarization values for these pillar heights are computed, respectively, as 0.57, 0.45, and 0.35, thus suggesting that an effective coupling between in- and out-of-plane motion can be expected for narrower frequency ranges as the pillar height increases. Upon illumination, the softening of the material of the pillars (whose Young's modulus changes to approximately 2.0 GPa for maximum illumination power) leads to a lowering of the propagating frequencies at  $\Gamma$  to the new values of (i) 38.5, (ii) 28.7, (iii) 22.1, and (iv) 17.5 kHz, thus corresponding to an approximate decrease of 15% from the initial values of these frequencies.

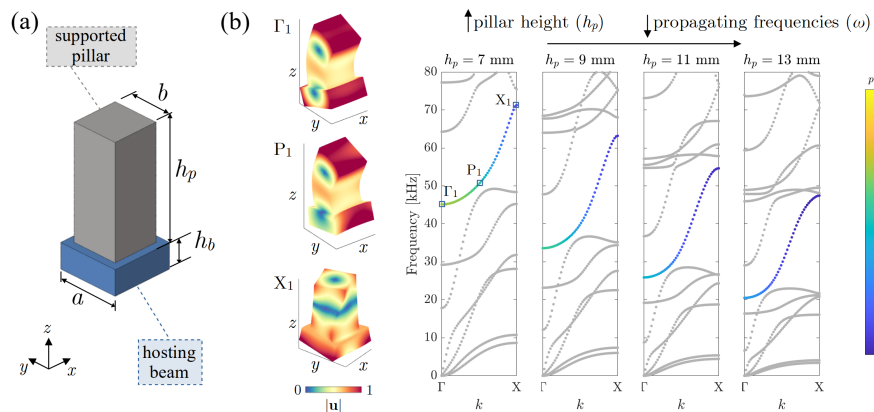


Figure 2: Dispersion properties of the photo-responsive pillars. (a) The characteristic dimensions of the unit cell are described by a hosting beam with base width  $a$  and height  $h_b$ , supporting a pillar with width  $b$  and height  $h_p$ . (b) Dispersion relations computed for the values  $h_p = \{7, 9, 11, 13\}$  mm. The polarization metric ( $p$ ), computed considering the hosting beam volume, is used to indicate the behavior of a branch supporting flexural waves whose behavior shifts between the wave modes shown at the lower ( $\Gamma_1$ ) and upper ( $X_1$ ) points, indicating a highly coupled in- and out-of-plane behavior for intermediate values, and hence reduced transmission. Vibration modes at the points  $\Gamma_1$ ,  $P_1$  and  $X_1$  are also shown on the left of the subfigure.

We now numerically model the finite structure considered experimentally (Fig.3a), constituted by the described pillars arranged in a one-dimensional array on a thin beam (40 mm in length, 2 mm in thickness) acting as a waveguide, located between a 40x40 mm slab used to excite input signals and a 40x4.5 mm beam where output signals are detected. To reinforce the locally resonant effect of each pillar, each height is repeated twice, leading to an 8-pillar structure, whose collective transmission properties are approximately expected to be the superposition of those of the four individual pillar types. This is based on the assumption of limited coupling between vibration modes of the various pillars in the considered frequency range.

To verify this hypothesis and determine the structure's overall transmission properties, we perform FEM frequency-domain numerical analysis using the COMSOL Multiphysics software. The finite structure geometry is reproduced and meshed using tetrahedral elements, as shown in (Fig.3b). Mechanical properties are those indicated above. A harmonic boundary load is applied on one side of the waveguide (corresponding to the location of the piezoelectric transducer in experiments), as shown in (Fig.3b), and the corresponding transmission loss (calculated as the ratio between transmitted and input power for out-of-plane vibrations) is then evaluated at the beam location opposite to the pillar array (also indicated in (Fig.3b)), in the 10 to 70 kHz range. Pillar illumination is simulated by locally reducing the Young's modulus to 2 GPa.

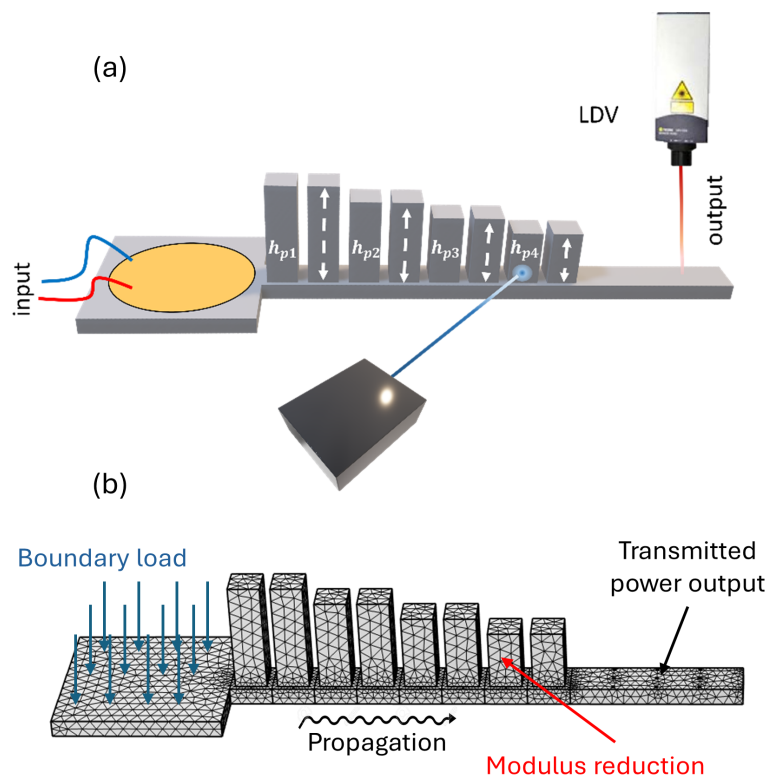


Figure 3: a) Experimental sample and measurement set-up. The heights of the pillars are  $h_{p1} = 13$  mm,  $h_{p2} = 11$  mm,  $h_{p3} = 9$  mm, and  $h_{p4} = 7$  mm. b) FEM mesh used in frequency-domain simulations; boundary conditions are also illustrated.

The computed spectrum (blue continuous line in Fig.4(a)) clearly shows the presence of four band gaps, appearing approximately in the frequency ranges predicted in the dispersion spectra (see Fig.2). Some variation in the band gap width is observed, mainly due to coupling effects between pillars. The effect of laser illumination at selected locations of the sample is then

evaluated. As an example, we consider the case when the 1st (4(a)) and 6th (4(b)) pillars are illuminated. In the first case, the pillar resonance frequency is related to the lowest band gap (I), at about 25 kHz. Figure 4(a) illustrates the variation in the transmission spectrum (red dashed line) upon softening of the first pillar, with the lowest band gap widening to lower frequencies (highlighted by red shading in the figure). In the second case, the sixth pillar is associated to the third band gap (III) at about 42 kHz, which undergoes widening and a shift to lower frequencies when the pillar undergoes softening (Fig.4(b)).

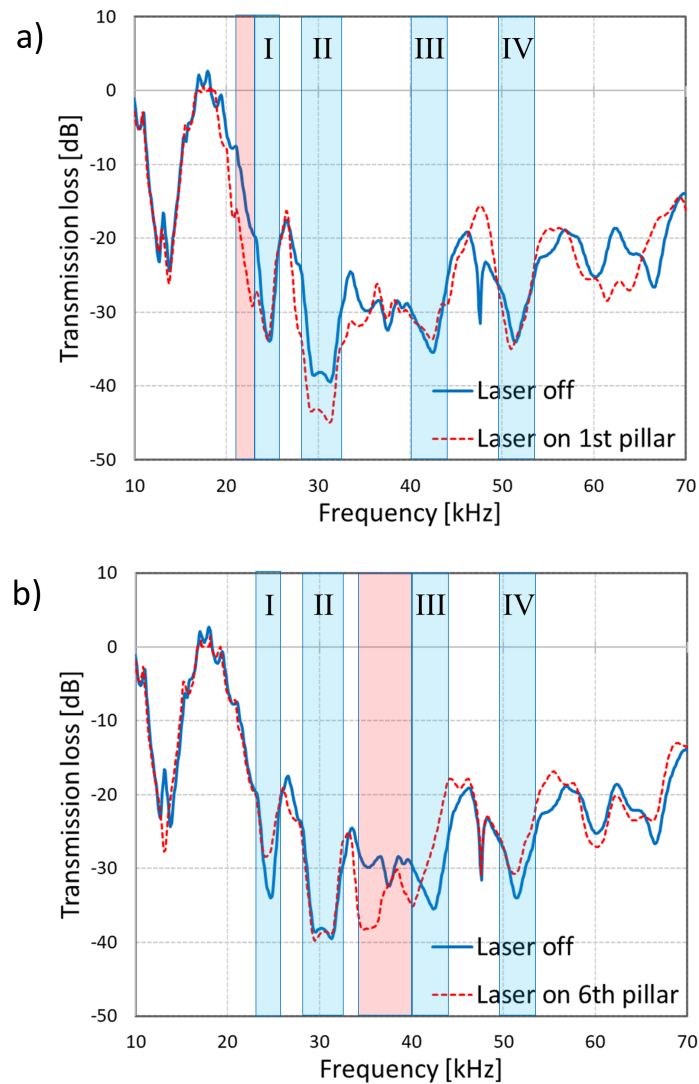


Figure 4: Numerically computed transmission spectrum of the considered 8-pillar structure. a) without ("Laser off") and with laser illumination on the first pillar ("Laser on 1st pillar"). Four band gaps (shaded in light blue and labelled from I to IV) appear in the spectrum; laser illumination on the tallest pillar results in a widening of the lowest bandgap to lower frequencies (red shading). b) without ("Laser off") and with laser illumination on the sixth pillar ("Laser on 6th pillar"). This results in a widening and lowering of the third band gap to lower frequencies (red shading).

### 3 Experimental realization

We now verify the numerical results through experimental tests. For the fabrication of the light-responsive specimen we follow a protocol described in [46]. The samples are first fabricated with a Digital Light Processing (DLP) 3D printer, using a commercial polymeric resin. Light-mediated tunability is then achieved by diffusing the responsive azo-dye Disperse Red 1 methacrylate (DR1m) into the as-fabricated samples prior to UV post-curing. Process parameters are selected so as to maximize homogeneous dye dispersion while preserving the integrity of the structure. The modulus of the material can thus be locally altered through illumination with visible light, producing continuous photo-isomerization cycles of the dye.

The experimental setup shown in Fig.3(a) is designed to detect the collective dynamics of the graded pillar structure. One side of the thin slab is designed to accommodate a thin piezoelectric transducer, whose mass is considered negligible. The transducer serves as the mechanical excitation source, generating elastic waves that propagate along the **beam** waveguide, crossing the array of pillars with varying heights, starting from the highest. The collective response of the structure is monitored by measuring the spectral response at the opposite end of the waveguide using a Laser Doppler Vibrometer (LDV). An additional laser, operating at a wavelength of  $\lambda = 405$  nm, is positioned orthogonally to the structure on a motorized linear stage. This allows to selectively illuminate individual pillars (see Fig.3(a)).

To explore the frequency response of the structure, we perform a frequency sweep ranging from 10 kHz to 70 kHz, capturing the system's response using the LDV to monitor the output of the structure and performing Fast Fourier Transform Analysis to determine the transmitted spectrum. The results reveal, as expected, the emergence of four distinct bandgaps, each characterized by an increasing width for increasing frequencies. These bandgaps correspond to the lower bandgaps of each pillar pair (as illustrated in Fig.4(a), solid blue line). The central frequencies of these bandgaps align well with the positions predicted from the modal analysis of individual pillars and with those calculated in frequency domain simulations. As the frequency increases, there is a slight deviation between the experimental data and the predictions, due to the mentioned excitation of in-plane modes and coupling effects between pillars.

The subsequent phase of the experiments involves the selective illumination of the structure at selected locations. Fig.4(a) shows results when illuminating the first (tallest) pillar, responsible for the formation of the lowest frequency bandgap. The illumination induces a reduction of the elastic modulus in the illuminated pillar, resulting in a resonance frequency shift and a corresponding broadening of the first bandgap towards lower frequencies, **as predicted numerically**. In this case, only one of the two identical adjacent pillars undergoes a modification in its elastic behavior. At the edge of the first bandgap, this translates into a substantial difference in signal transmission of approximately 20dB at approximately 23 kHz before and after illumination. This illustrates the significant potential of the photo-induced modulation of material properties in modifying the structural response at specific frequencies, providing clear evidence of the tunable nature of the considered graded pillar metamaterial structure. Illumination of the first pillar also produces noticeable effects at other frequencies in the spectral response, due to the effect on the modification of higher modes (Fig.4(a), red line). The temporal evolution of the entire structure's elastic response is visually represented in the color map presented in Fig.4(b), with time depicted on the vertical axis. The illumination of the pillar begins after 700 seconds (lower horizontal white line), reaching a steady state approximately 150 seconds later. Subsequently, the structure returns to its initial state in roughly the same time interval after the laser is switched off (upper horizontal line in the map), demonstrating full reversibility of the process.

Similar effects are observed **for the other case considered in simulations, i.e.**, when illuminating the sixth pillar in the array, which is responsible for opening the third bandgap. In this instance, the softening of the structure appears to have more pronounced effects, partly because the illuminated area covers a larger percentage of the pillar volume (Fig.4(c)). As a result, the second and third bandgaps combine, while the response at other frequencies remains relatively unchanged (Fig.4(d)). This dynamic response further emphasizes the versatility of the

graded pillar structure in achieving tunable and selective control over specific frequency ranges, illustrating its potential for targeted reversible modulation in applications requiring tailored dynamic behavior.

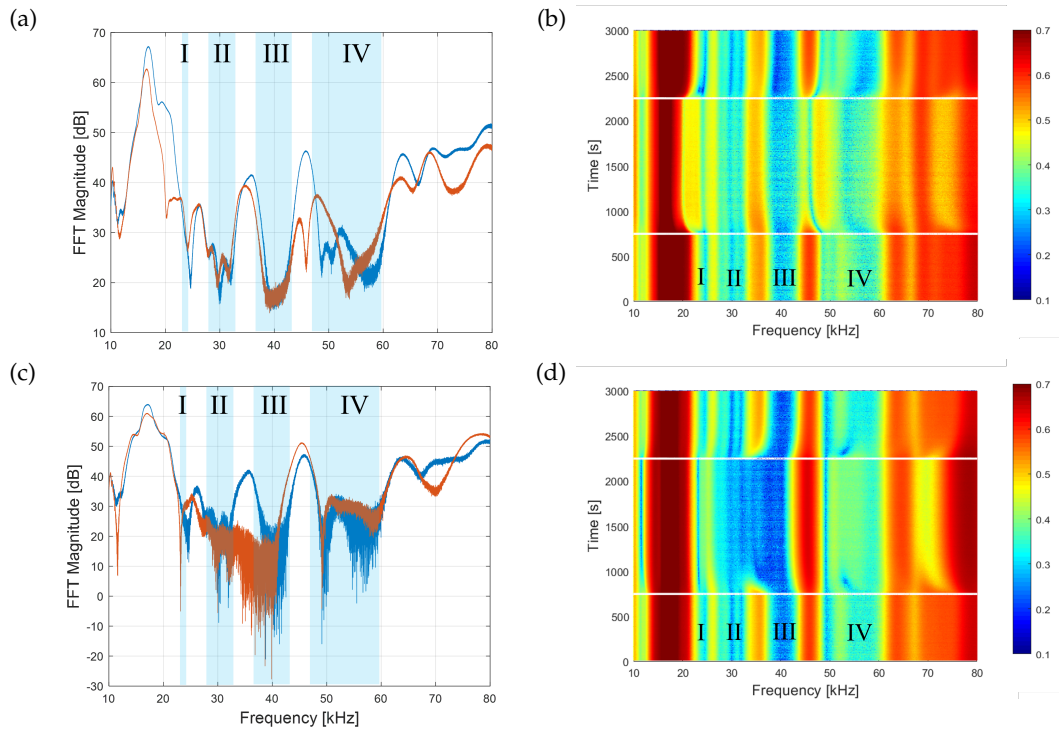
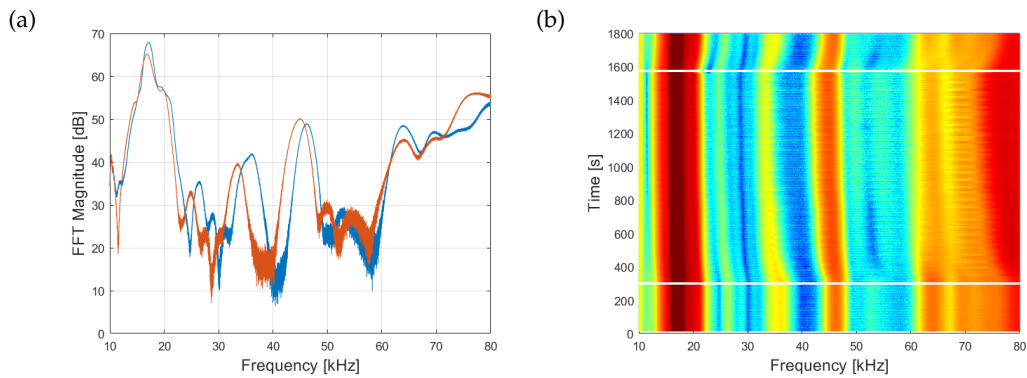


Figure 5: Transmission spectrum of the finite structure considered experimentally. a) Measured spectra before (blue) and after (red) illumination of pillar 1. Band gaps are highlighted in light blue and numbered from I to IV; b) Corresponding colour map representing transmission vs. frequency and time (vertical axis) when switching laser illumination on ( $t = 700$  s) and off ( $t = 2300$  s); c) same as a), with illumination of pillar 6; d) same as b), with illumination on pillar 6.

In addition to the experiments involving illumination of individual photoresponsive pillars, we explored the possibility of simultaneously illuminating multiple or all pillars in the system. We illustrate here the latter case. For this experiment, a laser was mounted on a linear stage, allowing the light beam to traverse back and forth across the array of pillars. Due to the inherent time delay in photoresponsive material property modification (a finite time is required to activate/deactivate the photo-isomerization), the continuous movement of the laser is effectively equivalent to quasi-simultaneous illumination of all pillars. As expected, the collective effect of simultaneously illuminating all pillars results in the cumulative effect of individual illuminations, in this case manifesting itself as a rigid spectral shift toward lower frequencies across the entire spectrum, as shown in Fig.6. The possibility to manipulate the optical response of multiple elements simultaneously highlights the versatility of our system.

Finally, we explore a practical application. Specifically, we inject a composite signal comprising two frequencies,  $f_1 = 21.5$  kHz and  $f_2 = 71.5$  kHz changing the selective laser illumination of the sample in time to observe the change in spectral response, as illustrated in Fig.7. During the first phase (from  $t_0 = 0$  to  $t_1 = 50$  s), none of the pillars are illuminated, resulting in both frequencies exhibiting comparable spectral weights. Subsequently, at  $t_1$ , we selectively illuminate the fourth pillar. This action induces a local softening of the structure, effectively suppressing  $f_2$  and causing a slight increase in  $f_1$ . Subsequently, the laser is switched off (from  $t_2 = 100$  s to



**Figure 6:** Transmission spectrum of the finite structure considered experimentally. a) Measured spectra before (blue) and after (red) illumination of all pillars simultaneously. A rigid down-shift of the whole spectrum is observed; b) Corresponding colour map representing transmission vs. frequency and time (vertical axis) when switching laser illumination on ( $t = 300$  s) and off ( $t = 1600$  s).

$t_3 = 150$ s), so that the system returns to its initial state. Finally, in the last phase (from  $t_3$  onwards), we illuminate the first pillar. This leads to a selective softening of this pillar, resulting in a significant amplitude reduction of  $f_1$  in favour of  $f_2$ . The relative spectral weights of the two frequencies thus become fully modifiable, offering a dynamic and reversible means of controlling signal components within the structure. This provides an example of how the tunable graded pillar structures can be used to actively modulate the spectral characteristics of injected signals.

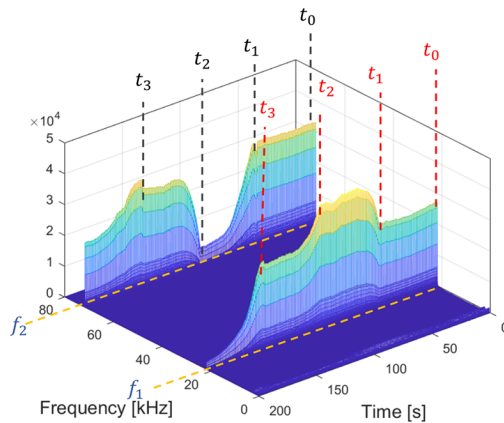


**Figure 7:** Dynamic modulation of signal frequencies ( $f_1 = 21.5$  kHz,  $f_2 = 71.5$  kHz) in a graded pillar structure. The different temporal intervals depict tunable suppression and enhancement of specific frequencies through selective pillar illumination.

## 4 Conclusion

In conclusion, we have shown how it is possible to exploit graded locally resonant structures in conjunction with light-responsive polymers to obtain metamaterials with multiple degrees of freedom of dynamic tunability. The selective modulation of the elastic properties of a photosensitive polymer by means of laser illumination provides a controlled and reversible

means to manipulate the elastic characteristics of the waveguide. The spatial arrangement of pillars, each acting as a different resonator, provides a rich platform to explore the interplay between static and dynamic gradings. In this sense, we can compare this system to a piano keyboard, where the activation of different key combinations produces various note sequences, or melodies, in output. In our case, the analogy is between pillars and piano keys, and between laser illumination and finger pressure on the keys. As in the case of a piano keyboard, key combinations can be used to obtain combinations of output frequencies, or tones. Preliminary experiments on even a relatively simple structure (8 pillars of 4 different heights) indicate that due to the complex resonant behaviour of the pillars and their coupling, there is rarely a one to one relation between illumination of a single pillar and shift of a single band gap. Thus, to use such a "metamaterial keyboard" in applications, an accurate "map" of the frequency output needs to be determined, either numerically or experimentally. This will be the subject of future investigations.

Our work adds to other advances in metamaterial research that address the challenge of dynamic tunability, which allows to go beyond traditional metamaterials. Our approach introduces one possible avenue for achieving this dynamic control over elastic wave manipulation. The ability to selectively tune and suppress specific frequencies over time opens possibilities for innovative applications, particularly in dynamic signal processing, where tailored frequency responses are crucial. This is of particular relevance in active devices for elastic wave control, such as beam-splitters, switches, and filters.

**Acknowledgements.** V.F.D.P., F.N., P.H.B., M.M., N.M.P., F.B and A.S.G. are supported by the European Commission H2020 FET Open "Boheme" grant no. 863179. F.N. is grateful to the Cassa di Risparmio di Torino foundation for support

## References

1. P. A. Deymier, *Acoustic Metamaterials and Phononic Crystals*, Springer Berlin, Heidelberg (2013).
2. R. V. Craster, S. Guenneau, *Acoustic Metamaterials: Negative Refraction, Imaging, Lensing and Cloaking*, Springer Science+Business Media Dordrecht (2013).
3. A. O. Krushynska, D. Torrent, A. M. Arag3n, R. Ardito, O. R. Bilal, B. Bonello, F. Bosia, Y. Chen, J. Christensen, A. Colombi, S. A. Cummer, B. Djafari-Rouhani, F. Fraternali, P. I. Galich, P. D. Garcia, J. P. Groby, S. Guenneau, M. R. Haberman, M. I. Hussein, S. Janbaz, N. Jim3nez, A. Khelif, V. Laude, M. J. Mirzaali, P. Packo, A. Palermo, Y. Pennec, R. Pic3, M. R. L3pez, S. Rudykh, M. Serra-Garcia, C. M. S. Torres, T. A. Starkey, V. Tournat, O. B. Wright, Emerging topics in nanophononics and elastic, acoustic, and mechanical metamaterials: an overview, *Nanophotonics*, 12 (4), pp. 659-686 (2023).
4. M.J. Hussein, M.J. Leamy, & M. Ruzzene, Dynamics of Phononic Materials and Structures: Historical Origins, Recent Progress, and Future Outlook. *Applied Mechanics Reviews*, 66, 040802 (2014).
5. M. Mazzotti, A. Foehr, O.R. Bilal, A. Bergamini, F. Bosia, C. Daraio, N.M. Pugno & M. Miniaci, Bio-inspired non self-similar hierarchical elastic metamaterials, *International Journal of Mechanical Sciences*, 41, pp. 107915 (2023).
6. Z. Liu, X. Zhang, Y. Mao, Y. Zhu, Z. Yang, C. Chan, P. Sheng, Locally resonant sonic materials., *Science*. 289, 1734-1736 (2000)
7. V. Romero-García, G. Theocharis, O. Richoux, A. Merkel, V. Tournat, V. Pagneux, Perfect and broadband acoustic absorption by critically coupled sub-wavelength resonators. *Scientific Reports*. 6, 19519 (2016)
8. N. Kaina, F. Lemoult, M. Fink, G. Lerosey, Negative refractive index and acoustic superlens from multiple scattering in single negative metamaterials. *Nature*. 525, 77-81 (2015)
9. L. Zigoneanu, B. Popa, S. Cummer, Three-dimensional broadband omnidirectional acoustic ground cloak. *Nature Materials*. 13, 352-355 (2014)
10. J. Pendry, Negative refraction makes a perfect lens. *Physical Review Letters*. 85, 3966 (2000)
11. A. Gliozzi, M. Miniaci, A. Krushynska, B. Morvan, M. Scalerandi, N. Pugno, F. Bosia, Proof of concept of a frequency-preserving and time-invariant metamaterial-based nonlinear acoustic diode. *Scientific Reports*. 9, 9560 (2019)

12. Zhang, X., Xiao, M., Cheng, Y., Lu, M. & Christensen, J. Topological sound. *Communications Physics*. **1**, 97 (2018)
13. S. Mousavi, A. Khanikaev, Z. Wang, Topologically protected elastic waves in phononic metamaterials. *Nature Communications*. **6**, 8682 (2015)
14. A. Colombi, D. Colquitt, P. Roux, S. Guenneau, R. Craster, A seismic metamaterial: The resonant metawedge. *Scientific Reports*. **6**, 27717 (2016)
15. A. Palermo, S. Krödel, A. Marzani, C. Daraio, Engineered metabarrier as shield from seismic surface waves. *Scientific Reports*. **6**, 1-10 (2016)
16. M. Miniaci, A. Krushynska, F. Bosia, N. Pugno, Large scale mechanical metamaterials as seismic shields. *New Journal Of Physics*. **18**, 083041 (2016)
17. J. De Ponti, A. Colombi, R. Ardito, F. Braghin, A. Corigliano, R. Craster, Graded elastic metasurface for enhanced energy harvesting. *New Journal Of Physics*. **22**, 013013 (2020)
18. N. Jiménez, V. Romero-García, V. Pagneux, J. Groby, Rainbow-trapping absorbers: Broadband, perfect and asymmetric sound absorption by subwavelength panels for transmission problems. *Scientific Reports*. **7**, 13595 (2017)
19. N. Gao, Z. Zhang, J. Deng, X. Guo, B. Cheng, H. Hou, Acoustic metamaterials for noise reduction: a review. *Advanced Materials Technologies*. **7**, 2100698 (2022)
20. T. Dubček, D. Moreno-Garcia, T. Haag, P. Omidvar, H. Thomsen, T. Becker, L. Gebraad, C. Bärlöcher, F. Andersson, S. Huber, Others In-Sensor Passive Speech Classification with Phononic Metamaterials. *Advanced Functional Materials*. pp. 2311877 (2024)
21. F. Casadei, M. Ruzzene, L. Dozio, K. A. Cunefare, Broadband vibration control through periodic arrays of resonant shunts: experimental investigation on plates, *Smart Mat. and Struct.*, **19** (1), 015002 (2010).
22. A. Bergamini, T. Delpero, L. D. Simoni, L. D. Lillo, M. Ruzzene, P. Ermanni, Phononic crystal with adaptive connectivity, *Adv. Mat.*, **26** (9), 1343–1347 (2014).
23. N. Kherraz, L. Haumesser, F. Levassort, P. Benard, B. Morvan, Controlling Bragg gaps induced by electric boundary conditions in phononic piezoelectric plates, *Appl. Phys. Lett.*, **108** (9), 093503 (2016).
24. L. Airoldi, M. Ruzzene, Design of tunable acoustic metamaterials through periodic arrays of resonant shunted piezos, *New J. Phys.*, **13** (11) 113010 (2011).
25. X. Guo, P. Wei, Dispersion relations of elastic waves in one-dimensional piezoelectric/piezomagnetic phononic crystal with initial stresses, *Ultrasonics*, **66**, 72–85 (2016).
26. K. L. Jim, C. W. Leung, S. T. Lau, S. H. Choy, H. L. W. Chan, Thermal tuning of phononic bandstructure in ferroelectric ceramic/epoxy phononic crystal, *Appl. Phys. Lett.*, **94**, 193501 (2009).
27. Y. Cheng, X. J. Liu, D. J. Wu, Temperature effects on the band gaps of Lamb waves in a one-dimensional phononic-crystal plate (L), *J. Acoust. Soc. Am.*, **129** (3), 1157–1160 (2011).
28. W. Lewandowski, M. Fruhnert, Mieczkowski, C. Rockstuhl, E. Górecka, Dynamically self-assembled silver nanoparticles as a thermally tunable metamaterial, *Nat. Commun.*, **6**, 6590 (2015).
29. C. Goffaux, J. Vigneron, Theoretical study of a tunable phononic band gap system, *Phys. Rev. B*, **64** (7), 075118 (2001).
30. B. Florijn, C. Coulais, M. van Hecke, Programmable mechanical metamaterials, *Phys. Rev. Lett.*, **113** (17), 175503 (2014).
31. M. Miniaci, M. Mazzotti, A. Amendola, F. Fraternali, Effect of prestress on phononic band gaps induced by inertial amplification. *International Journal Of Solids And Structures*. **216** pp. 156-166 (2021)
32. M. Morvaridi, F. Bosia, M. Brun, V. Dal Poggetto, A. Gliozzi, M. Miniaci, C. Croënne, N. Pugno, G. Carta, Tunable topologically protected waveguiding in auxetic nonlinear metamaterials. *Physical Review Applied*. **21**, 034024 (2024)
33. J.-F. Robillard, O. Bou Matar, J. Vasseur, P. A. Deymier, M. Stippinger, A.-C. Hladky-Hennion, Y. Pennec, B. Djafari-Rouhani, Tunable magnetoelastic phononic crystals, *Appl. Phys. Lett.*, **95** (12), 124104 (2009).
34. Z. Xu, F. Wu, Z. Guo, Shear-wave band gaps tuned in two-dimensional phononic crystals with magnetorheological material, *Solid State Commun.*, **154**, 43–45 (2013).
35. Y. G. S. Zhang, Y. Shi, Tunability of band structures in a two-dimensional magnetostrictive phononic crystal plate with stress and magnetic loadings, *Phys. Lett. A*, **381** (12), 1055 – 1066 (2017).

36. B.-I. Popa, L. Zigoneanu, S. A. Cummer, Tunable active acoustic metamaterials, *Phys. Rev. B*, **88** (2), 024303 (2013).
37. E. Walker, D. Reyes, M. M. Rojas, A. Krokhnin, Z. Wang, A. Neogi, Tunable ultrasonic phononic crystal controlled by infrared radiation, *Appl. Phys. Lett.*, **105** (14), 143503 (2014).
38. E. L. Walker, Z. Wang, A. Neogi, Radio-frequency actuated polymer-based phononic metamaterials for control of ultrasonic waves, *NPG Asia Mater.* **9** (2), e350 (2017).
39. A. Goshkoderia, V. Chen, J. Li, A. Juhl, P. Buskohl, S. Rudykh, Instability-Induced Pattern Formations in Soft Magnetoactive Composites, *Physical Review Letters*, **124**, 158002 (2020)
40. N. Arora, V. Chen, A. Cherkasov, Y. Xiang, A. Juhl, P. Buskohl, S. Rudykh, Magnetically-Programmed Instability-Driven Pattern Transformations in Soft Materials, *Advanced Functional Materials*, 2401077 (2024)
41. M. R. O'Neill, D. Sessions, N. Arora, V. W. Chen, A. Juhl, G. H. Huff, S. Rudykh, R. F. Shepherd, P. R. Buskohl, Dielectric Elastomer Architectures with Strain-Tunable Permittivity. *Adv. Mater. Technol.*, **7**, 2200296 (2022)
42. Y. Xue, J. Li, Y. Wang, Z. Song, A. O. Krushynska, Widely tunable magnetorheological metamaterials with nonlinear amplification mechanism, *International Journal of Mechanical Sciences*, **264**, 108830 (2024)
43. M. Pishvar and R. L. Harne, Foundations for Soft, Smart Matter by Active Mechanical Metamaterials, *Advanced Science*, **7**, 200138 (2020)
44. A. S. Gliozzi, M. Miniaci, A. Chiappone, A. Bergamini, B. Morin, and E. Descrovi, Tunable photo-responsive elastic metamaterials, *Nat. Commun.* **11**, 2576 (2020).
45. I. Roppolo, A. Chiappone, A. Angelini, S. Stassi, F. Frascella, C.F. Pirri, C. Ricciardi, C., E. Descrovi, 3D printable light-responsive polymers. *Mater. Horiz.* **4**, 396–401 (2017).
46. G. J. Chaplain, A. S. Gliozzi, B. Davies, D. Urban, E. Descrovi, F. Bosia, R. V. Craster, Tunable topological edge modes in Su–Schrieffer–Heeger arrays, *Appl. Phys. Lett.* **122**, 221703 (2023)
47. B. R. Mace, E. Manconi, “Modelling wave propagation in two-dimensional structures using finite element analysis,” *Journal of Sound and Vibration*, vol. 318(4-5), pp. 884-902, 2008.
48. L. Brillouin, “Wave propagation in periodic structures; electric filters and crystal lattices,” *K Courier Dover Publications* 1946.
49. Miniaci, M., Gliozzi, A., Morvan, B., Krushynska, A., Bosia, F., Scalerandi, M. & Pugno, N. Proof of concept for an ultrasensitive technique to detect and localize sources of elastic nonlinearity using phononic crystals. *Physical Review Letters*. **118**, 214301 (2017)